

Article

Single-Crystal Structure Analysis of Dicarboxamides: Impact of Heteroatoms on Hydrogen Bonding of Carboxamide Groups

Abdulrahman Mohabbat , Jasmin Salama, Philipp Seiffert , István Boldog and Christoph Janiak * 

Institut für Anorganische Chemie und Strukturchemie, Heinrich-Heine-Universität, 40204 Düsseldorf, Germany; abdulrahman.mohabbat@uni-duesseldorf.de (A.M.); jasmin.salama@uni-duesseldorf.de (J.S.); philipp.seiffert@uni-duesseldorf.de (P.S.); boldogi@uni-duesseldorf.de (I.B.)

* Correspondence: janiak@uni-duesseldorf.de

Abstract: This research examines how heteroatoms in a six- or five-membered pyridine, thiophene or furan ring spacer between two carboxamide groups influence the hydrogen bonding for advancements in supramolecular chemistry and drug development. The solvent-free crystal structures of 3,5-pyridinedicarboxamide (PDC), 2,5-thiophenedicarboxamide (TDC) and 2,5-furandicarboxamide (FDC-subl, crystallized by sublimation), and the monohydrate structure of FDC-solv (crystallized from methanol) are described with the hydrogen-bonding analyzed by the Etter graph-set notation. The carbon atoms of the amide groups form an angle of 121° in PDC, 151° in TDC, 137° in FDC-solv and 135° in FDC-subl with the ring centroid. Only in the structure of PDC does the heteroatom act as an H-bond acceptor as part of a C₁¹(6) chain. In TDC and FDC, the heteroatoms do not interact with the amide -NH₂ groups.

Keywords: dicarboxamides; hydrogen bonding; Etter graph set; heteroatoms



Citation: Mohabbat, A.; Salama, J.; Seiffert, P.; Boldog, I.; Janiak, C. Single-Crystal Structure Analysis of Dicarboxamides: Impact of Heteroatoms on Hydrogen Bonding of Carboxamide Groups. *Crystals* **2024**, *14*, 811. <https://doi.org/10.3390/cryst14090811>

Academic Editor: Maciej Kubicki

Received: 5 August 2024

Revised: 4 September 2024

Accepted: 9 September 2024

Published: 14 September 2024



Copyright: © 2024 by the authors. Licensee MDPI, Basel, Switzerland. This article is an open access article distributed under the terms and conditions of the Creative Commons Attribution (CC BY) license (<https://creativecommons.org/licenses/by/4.0/>).

1. Introduction

The amide group (R-C(=O)-NH-R') is an essential functional synthon and contributes significantly to the functionality of biologically relevant compounds, including peptides, proteins and active pharmaceutical ingredients [1]. The amide bond has become increasingly important in drug design and development. Several top-selling drugs contain an amide functional group as part of their pharmacophore or auxophore [2]. The functionality of the amide group is due to its role in the formation of hydrogen bonds [3]. For example, amide groups are used in the pharmaceutical industry to engage an active pharmaceutical ingredient with a cofomer or to modify drug properties [4]. In order to transport the pharmaceutical ingredient to the desired location and achieve the intended effect, drug delivery systems have become established in many medical fields [5,6]. These systems increase efficacy, control the release of the active ingredient and reduce the required dose [7]. Moreover, amides have additional applications in coordination chemistry [8], playing a crucial role in stabilizing reactive species or used for sensing applications, particularly in the development of fluorescent and colorimetric sensors with high selectivity and sensitivity for the detection of heavy metal ions [9,10]. In this context, research into supramolecular interactions is crucial to understand the relationships between materials, drugs and organisms and to advance the development of these systems [11–15].

Research in the field of supramolecular chemistry focuses on the construction of complex chemical systems by using hydrogen bonds [16]. Due to the directionality of non-covalent hydrogen bonds, they significantly influence phenomena such as crystal growth and the structural stabilization of proteins and thus the physical properties of the materials [17]. The use of so-called supramolecular synthons is a common approach here. Synthons have molecular complementarity and occur either between identical functional groups (homosynthons) or between non-identical functional groups (heterosynthons).

Hydrogen bonds occur when a hydrogen atom attached to an electronegative atom (D) interacts with a second electronegative atom (A) to form a D-H...A contact [17]. The electrostatic interaction between the H-bond donor (D-H) and the acceptor atom (A) can occur between atoms within the same molecule (intramolecular) or between atoms in different molecules (intermolecular) [18,19]. An amide group typically contains two types of hydrogen bonds, where the carbonyl group acts as an acceptor and the NH group as a hydrogen bond donor [4].

A systematic approach to characterize hydrogen bonding between molecules was originally developed by M. C. Etter, who applied graph-set theory to identify patterns of hydrogen bonding and then used them to understand and design molecular crystals [20–22]. This notation is still commonly used in publications to describe hydrogen-bonding interactions [23–28]. Etter presented the combination of four basic patterns, each identified by a designator: chains (C), rings (R), intramolecular hydrogen bonds (S) and other finite patterns (D). The graph-set descriptor is specified according to the following syntax: $G_d^a(n)$, where G represents one of the four possible designators. A pattern is characterized by a subscript d for the number of hydrogen bond donors and a superscript a for the number of hydrogen bond acceptors. The number of atoms n in the pattern is given in brackets as the degree of the pattern [29] (Figure 1).

In crystals of primary amides, the orientation of the two H atoms of the primary amide NH_2 group can be differentiated as syn or anti to the carbonyl-O atom (Figure 1a). The H bonding interactions between amide–amide homosynthons can occur through complementary head-to-tail orientation and lead to the $R_2^2(8)$ ring hydrogen-bond motif, involving syn-oriented hydrogen atoms relative to the adjacent C=O bond (Figure 1b). Furthermore, the hydrogen bonding interaction between the C=O bond and the anti-oriented hydrogen atom results in the formation of the $C_1^1(4)$ chain hydrogen-bond motif (Figure 1c).

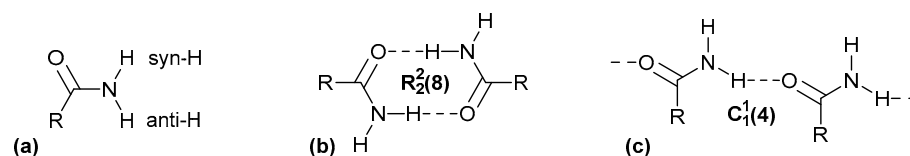


Figure 1. (a) Differentiation of the anti- and syn-H atom in primary amides. Classical hydrogen-bonding interactions between amide groups with the Etter notation for a ring (b) and chain (c) motif.

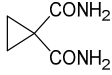
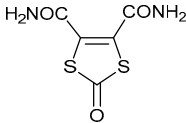
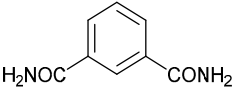
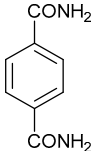
Hydrogen bonds can be classified into weak, strong and very strong hydrogen bonds based on their energetic properties and are shown in Table 1 [30].

Table 1. Classification of hydrogen bond strength.

Properties	Very Strong	Strong	Weak
Bond energy [kcal/mol]	15–40	4–15	<4
D...A [Å]	2.2–2.5	2.5–3.2	3.0–4.0
H...A [Å]	1.2–1.5	1.5–2.2	2.0–3.0
D-H...A [°]	175–180	130–180	90–180

Structurally authenticated primary dicarboxamides of small molecules have been extensively analyzed in terms of their packing modes with respect to the ideal hydrogen bonds of the amide groups and are shown in Table 2 [31].

Table 2. Literature examples of primary dicarboxamides of small molecules. The graph-set notation depicts only the level 1 units with the shortest rings and chains as calculated by Mercury [32].

Compounds	Name	Graph-Set	Reference
	Cyclopropane-1,1-dicarboxamide	$R_2^2(8)$ $C_1^1(6)$	[33]
	4,5-Dicarbamoyl-1,3-dithiol-2-one	$R_2^2(8)$ $C_1^1(7)$ $R_2^2(14)$	[34]
	1,3-Benzenedicarboxamide	$R_2^2(8)$ $C_1^1(4)$	[35]
	Terephthalamide	$R_2^2(8)$ $C_1^1(9)$ $C_1^1(4)$	[36]

To the best of our knowledge, the earliest reports on synthesis of the dicarboxamides, which were investigated in our study, are for 3,5-pyridinedicarboxamide (PDC) by Meyer et al. [37], for 2,5-thiophenedicarboxamide (TDC) by Oussaid et al. [38] and for FDC by Klinkhardt [39]. In these pioneering studies, the synthesis routes were described, and the melting points and solubility properties of these compounds were investigated. Surprisingly, the solid-state crystal structures of the dicarboxamides 3,5-pyridinedicarboxamide (PDC), 2,5-thiophenedicarboxamide (TDC) and 2,5-furandicarboxamide (FDC) had not yet been reported. Hence, we analyze their crystal structures to assess the influence of the heteroatoms in the aromatic ring spacer between the carboxamide groups on the formation of intermolecular hydrogen bonds between the carboxamide groups.

2. Materials and Methods

All chemicals were commercially obtained and were used without any further purification (see Supplementary Materials, Section S1). The water used was deionized.

FT-IR measurements were performed on a Bruker TENSOR 37 IR spectrometer (Bruker, Billerica, MA, USA) in ATR mode (Platinum ATR-QL, Diamond) in the range 500–4000 cm^{-1} . NMR measurements were carried out on a Bruker Avance III—300 (Bruker, Billerica, MA, USA) (^1H : 600 MHz; $^{13}\text{C}\{^1\text{H}\}$: 75 MHz). EI mass spectra were recorded using a Thermo Finnigan Trace DSQ spectrometer (Thermo Fisher Scientific, Waltham, MA, USA). Thermogravimetric analyses were performed on a Netzsch TG209 F3 Tarsus (Netzsch, Selb, Germany) in a synthetic air atmosphere with a ramp of 10 K min^{-1} up to 1000 $^\circ\text{C}$. Melting points were measured using a Büchi Melting Point B-540 apparatus (Büchi Labortechnik AG, Flawil, Switzerland). X-ray powder patterns were obtained by using a Rigaku Mini-Flex600 (Rigaku, Tokyo, Japan) (600 W, 40 kV, 15 mA) at room temperature with $\text{Cu-K}\alpha$ radiation ($\lambda = 1.54184 \text{ \AA}$). The highest reflex was normalized to 1, and the simulated powder patterns were derived from the single crystal data using MERCURY 2020.3.0 software [32].

Sublimation has proven to be an effective method for obtaining crystal polymorphs and to enable the (solvent-free) crystallization of compounds that are not accessible by other techniques [40]. In several cases, this method has led to the discovery of completely new solid-state (polymorphic) forms [41,42]. For this reason, the method was also employed in this work. The single crystal diffraction measurement for the materials were carried out on a Rigaku XtaLAB Synergy S diffractometer (Rigaku, Tokyo, Japan) with a hybrid pixel array detector and a micro-focus sealed X-ray tube, PhotonJet copper X-ray source ($\lambda = 1.54184 \text{ \AA}$).

The IR spectra of the dicarboxamides (see Supplementary Materials, Section S4) show the indicative bands for the characteristic CONH₂ band at around 1650 cm⁻¹ for δ(N-H) and 3050–3500 cm⁻¹ for ν(N-H).

3.1. Crystal Structures of the Dicarboxamides PDC, TDC, FDC-Solv and FDC-Subl

The solid-state crystal structures of the three dicarboxamides had not yet been investigated prior to our study. The compounds PDC, TDC and FDC-solv could be crystallized from methanol, whereas the crystals of FDC-subl were obtained by sublimation. The simulated powder X-ray diffraction patterns of the subsequently determined crystal structures were positively matched to the experimental powder patterns, which confirmed a high phase purity for the crystalline part of each compound (see Supplementary Materials, Section S6). The crystallographic parameters for the crystal structures of the dicarboxamides are given in Table 3.

Table 3. Crystal data for PDC, TDC and FDC.

	PDC	TDC	FDC-Solv	FDC-Subl
empirical formula	C ₇ H ₇ N ₃ O ₂	C ₆ H ₆ N ₂ O ₂ S	C ₆ H ₈ N ₂ O ₄	2(C ₆ H ₆ N ₂ O ₃)
mol wt (g mol ⁻¹)	165.16	170.19	172.14	308.26
temperature (K)	150	150	150	150
crystal system	monoclinic	monoclinic	monoclinic	monoclinic
space group	P2 ₁ /n	P2 ₁ /c	C2/c	P2 ₁ /c
a (Å)	3.7819 (1)	18.0336 (5)	7.4163 (1)	13.3086 (3)
b (Å)	15.3344 (7)	3.8429 (1)	12.8942 (2)	10.1634 (1)
c (Å)	12.1314 (5)	10.2084 (3)	7.8045 (1)	10.5981 (2)
α (deg)	90.00	90.00	90.00	90.00
β (deg)	96.023 (4)	102.507 (3)	96.290 (2)	106.399 (2)
γ (deg)	90.00	90.00	90.00	90.00
Volume, V (Å ³)	699.65 (5)	690.67 (3)	741.83 (2)	1375.19 (4)
Z, Z'	Z = 4, Z' = 1	Z = 4, Z' = 1	Z = 4, Z' = 1	Z = 8, Z' = 2
D _{calc} (g/cm ³)	1.568	1.637	1.541	1.489
μ (mm ⁻¹)	1.007	3.746	1.14	1.048
F(000)	344	352	360	640
crystal size [mm ³]	0.47 × 0.09 × 0.04	0.34 × 0.18 × 0.08	0.14 × 0.05 × 0.05	0.09 × 0.05 × 0.04
wavelength (Å)	1.54184	1.54184	1.54184	1.54184
No. of unique reflections	1284	13,941	2801	797
No. of total reflections	6472	13,941	16,323	23,894
No. of parameters	125	117	231	68
R _{int}	0.0789	– ^(c)	0.0306	0.0376
R ₁ [F ² > 2σ(F ²)] ^(a)	0.0603	0.0548	0.0323	0.0305
wR ₁ [F ² > 2σ(F ²)] ^(a)	0.1585	0.1725	0.0818	0.0846
R ₂ , wR ₂ (F ²) [all data] ^(a)	0.0669, 0.1651	0.0572, 0.1740	0.0390, 0.0858	0.0317, 0.0854
S [all data] ^(a)	1.111	1.148	1.047	1.081
Δρ _{max} , Δρ _{min} (e·Å ⁻³) ^(b)	0.39, 0.44	0.98, −0.69	0.15, −0.26	0.19, −0.21
CCDC no.	2374614	2374615	2374616	2374617

^(a) R₁ = [Σ(|F_o| − |F_c|)/Σ|F_o|]; wR₂ = [Σ[w(F_o² − F_c²)²]/Σ[w(F_o²)²]]^{1/2}. Goodness-of-fit S = [Σ[w(F_o² − F_c²)²]/(n − p)]^{1/2}. ^(b) Largest difference peak and hole. ^(c) This measurement is based on a non-merohedrally twinned structure. For non-merohedral twinning, data must not be merged, and therefore, the R_{int} value is not defined.

The three dicarboxamides crystallize in the monoclinic system. The molecular structures of the asymmetric unit are depicted in Figure 3. The pyridine dicarboxamides PDC have the space group $P2_1/n$, and the asymmetric unit consists of one molecule ($Z = 4$, $Z' = 1$). The thiophene and furan dicarboxamides TDC and FDC-subl have the same space group $P2_1/c$. In FDC-solv, the space group is $C2/c$, the dicarboxamide crystallizes with a water molecule and both the FDC molecule and the crystal water sit in a special position of the C_2 axis passing through O1 and O3. The asymmetric units of PDC, TDC and FDC-solv consist of one molecule ($Z = 4$, $Z' = 1$), but in the asymmetric unit of FDC-subl, two crystallographically independent forms are found ($Z = 8$, $Z' = 2$). It is also worth mentioning that the unit cell volume of FDC-subl ($V = 1375 \text{ \AA}^3$) is relatively large for this type of molecule. In contrast, the cell volumes of TDC ($V = 691 \text{ \AA}^3$), PDC ($V = 700 \text{ \AA}^3$) and FDC-solv ($V = 742 \text{ \AA}^3$) are comparable.

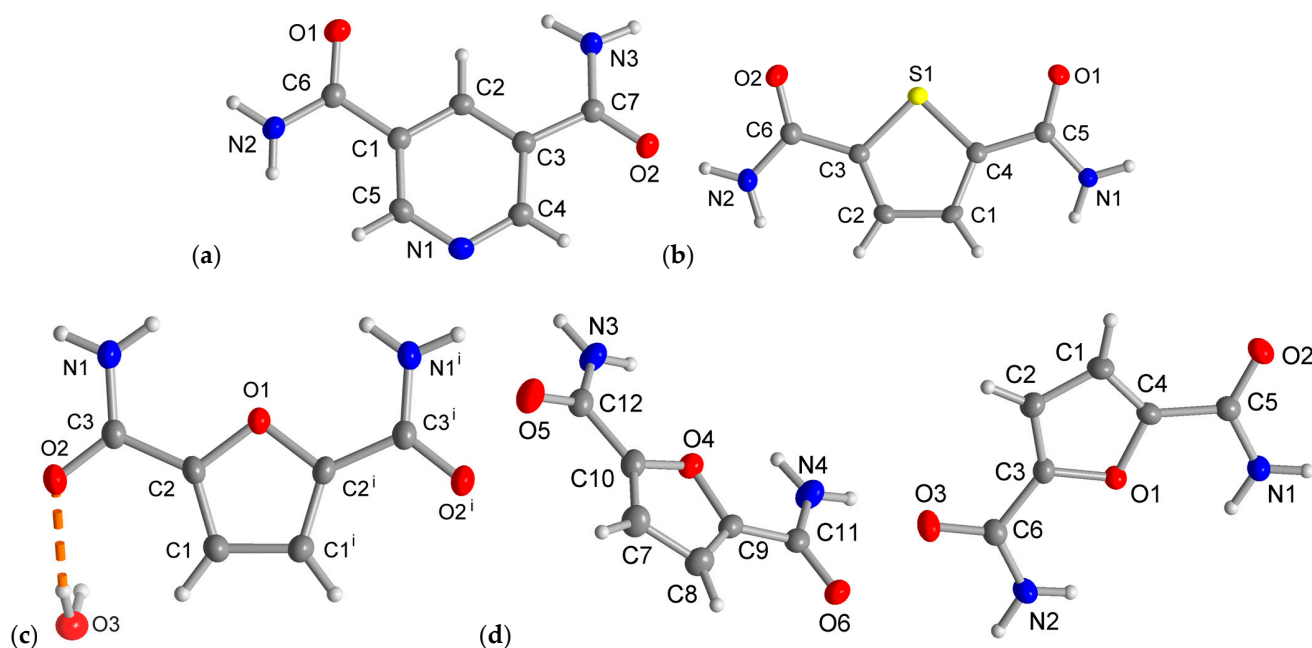


Figure 3. Asymmetric units with molecular structures of (a) PDC, (b) TDC, (c) FDC-solv and (d) FDC-subl (50% thermal ellipsoids, H atoms with arbitrary radii). Symmetry code for (c): (i) $-x + 2, y, -z + 1/2$.

The three dicarboxamides have an angular or V-shaped orientation of the two amide groups. The carbon atoms of the amide groups form an angle of 121° in PDC, 151° in TDC and 137° in FDC with the ring centroid (Figure 4). In their crystal structures, the orientation of the C=O and NH_2 part of the two amide groups is anti in PDC, syn-CO and syn- NH_2 in TDC and FDC. Therefore, in TDC the CO groups are on the side of the sulfur heteroatom, and in FDC the NH_2 groups are on the side of the oxygen heteroatom (Figure 4). This syn- NH_2 orientation to the furan-O atom may be brought about by long and strongly bent intramolecular $\text{N-H} \cdots \text{O}_{\text{furan}}$ bonds ($2.28\text{--}2.41 \text{ \AA}$, $102\text{--}106^\circ$). The syn- NH_2 orientation on the side of the heteroatom in FDC brings the NH_2 groups rather close together and enables a chelating-type $R_2^1(10)$ ring H-bonding interaction with an acceptor group (see below).

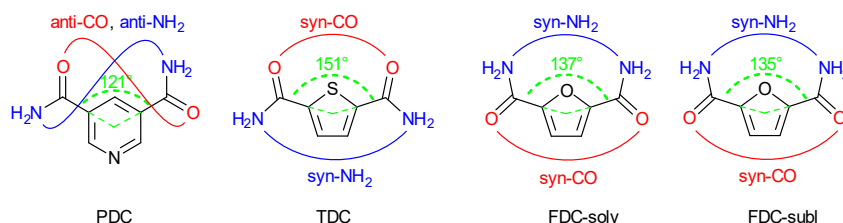


Figure 4. $C_{\text{amide}}\text{-centroid-}C_{\text{amide}}$ angle (in green) and syn/anti amide-CO (in red) and - NH_2 orientation (in blue) in PDC, TDC and FDC (both-solv and -subl).

3.2. Intermolecular Strong Hydrogen-Bonding Interactions of the Dicarboxamides

We will only present and discuss the N-H...O/N hydrogen bonds. These hydrogen bonds are at the upper limit of the strong H bonds (cf. Table 1). The structure of PDC is the only case among the three carboxamide structures where the heteroatom acts as an H-bond acceptor. The reason may be the basic nature and the open position of the pyridine-N atom in 3,5-pyridinedicarboxamide PDC, which is not flanked by the amide groups. In the analogous 2,6-pyridinedicarboxamide, with the amide groups adjacent to the pyridine-N atom, there are only two long and strongly bent intramolecular N-H...N_{py} bonds so that N_{py} does not accept intermolecular hydrogen bonds anymore [35]. In TDC, FDC-solv and FDC-subl the heteroatoms do not interact with the amide-NH₂ groups. Thus, N-H...X hydrogen bonds exist in these structures only between the amide groups and additionally between amide and crystal water in FDC-solv. The parameters for these strong hydrogen bonds are provided in Tables 4–7.

Table 4. Hydrogen bond parameters of the crystal structure of PDC.

<i>D</i> —H... <i>A</i> ^(a)	<i>D</i> —H [Å]	H... <i>A</i> [Å]	<i>D</i> ... <i>A</i> [Å]	<i>D</i> —H... <i>A</i> [deg]	Bond Energy [kcal/mol]
N2—H2A...O1 ⁱⁱ	0.93 (4)	1.88 (4)	2.810 (2)	177 (3)	−24
N2—H2B...O2 ⁱ	0.88 (4)	2.12 (4)	2.968 (2)	161 (4)	−12
N3—H3A...N1 ⁱⁱⁱ	0.93 (4)	2.16 (4)	3.033 (3)	156 (3)	−16
N3—H3B...O2 ^{iv}	0.92 (3)	2.08 (3)	2.978 (2)	165 (3)	−16

^(a) Symmetry codes: ⁱ $-x + 3/2, y - 1/2, -z + 3/2$; ⁱⁱ $-x, -y + 1, -z + 1$; ⁱⁱⁱ $x - 1/2, -y + 3/2, z - 1/2$; ^{iv} $-x + 2, -y + 2, -z + 1$.

Table 5. Hydrogen bond parameters of the crystal structure of TDC.

<i>D</i> —H... <i>A</i> ^(a)	<i>D</i> —H [Å]	H... <i>A</i> [Å]	<i>D</i> ... <i>A</i> [Å]	<i>D</i> —H... <i>A</i> [deg]	Bond Energy [kcal/mol]
N1—H1A...O1 ⁱⁱ	0.89 (5)	2.15 (5)	3.022 (5)	166 (4)	−12
N1—H1B...O1 ⁱⁱⁱ	0.87 (4)	2.08 (4)	2.944 (4)	172 (3)	−6
N2—H2A...O2 ⁱ	0.90 (7)	2.33 (7)	3.225 (5)	171 (4)	−8
N2—H2B...O2 ^{iv}	0.93 (5)	2.03 (5)	2.927 (4)	162 (4)	−15

^(a) Symmetry codes: ⁱ $x, -y + 3/2, z + 1/2$; ⁱⁱ $x, -y + 1/2, z + 1/2$; ⁱⁱⁱ $-x + 2, -y, -z + 1$; ^{iv} $-x + 1, y + 1/2, -z + 1/2$.

Table 6. Hydrogen bond parameters of the crystal structure of FDC-solv.

<i>D</i> —H... <i>A</i> ^(a)	<i>D</i> —H [Å]	H... <i>A</i> [Å]	<i>D</i> ... <i>A</i> [Å]	<i>D</i> —H... <i>A</i> [deg]	Bond Energy [kcal/mol]
N1—H1A...O3 ^{iv}	0.881 (16)	2.300 (16)	3.1799 (13)	176.7 (14)	−16
N1—H1B...O2 ^v	0.880 (18)	2.058 (19)	2.9269 (14)	169.2 (16)	−16
O3—H3...O2 ⁱⁱ	0.88 (2)	2.10 (2)	2.9395 (13)	160 (2)	−14

^(a) Symmetry codes: ⁱⁱ $-x + 1, y, -z + 1/2$; ^{iv} $x + 1/2, y + 1/2, z$; ^v $-x + 1, -y + 1, -z + 1$.

Table 7. Hydrogen bond parameters of the crystal structure of FDC-subl.

<i>D</i> —H... <i>A</i> ^(a)	<i>D</i> —H [Å]	H... <i>A</i> [Å]	<i>D</i> ... <i>A</i> [Å]	<i>D</i> —H... <i>A</i> [deg]	Bond Energy [kcal/mol]
N1—H1A...O2 ⁱ	0.895 (18)	2.286 (18)	3.1683 (14)	168.3 (15)	−8
N1—H1B...O6 ⁱⁱⁱ	0.882 (18)	2.026 (19)	2.9040 (14)	173.8 (16)	−17
N2—H2A...O6 ⁱⁱ	0.914 (19)	2.061 (18)	2.8498 (14)	143.7 (15)	−15
N2—H2B...O2 ⁱ	0.845 (18)	2.125 (19)	2.9545 (14)	167.3 (16)	−14
N3—H3A...O3 ^{iv}	0.903 (19)	1.974 (19)	2.8761 (15)	178.5 (16)	−19
N3—H3B...O5 ^v	0.904 (18)	2.270 (19)	3.1645 (15)	169.8 (15)	−8
N4—H4A...O5 ^v	0.893 (19)	2.269 (19)	3.1433 (16)	166.1 (16)	−9
N4—H4B...O3	0.90 (2)	1.95 (2)	2.8406 (14)	168.7 (18)	−18

^(a) Symmetry codes: ⁱ $-x + 2, y - 1/2, -z + 1/2$; ⁱⁱ $x, -y + 1/2, z - 1/2$; ⁱⁱⁱ $-x + 2, -y + 1, -z + 1$; ^{iv} $-x + 1, y + 1/2, -z + 3/2$; ^v $x, -y + 3/2, z - 1/2$.

The strong hydrogen bonds occurring in each dicarboxamide are shown and described using the Etter graph-set notation in Figures 5–8. The graph-set notation depicts only the level 1 units with the shortest rings and chains as calculated by Mercury [32].

The crystal structure of PDC consists of molecules held together by hydrogen-bonded $R_2^2(8)$ rings (Figure 5). Both symmetry independent amide groups form these $R_2^2(8)$ rings and in both cases to their inversion-symmetric counterparts. The N-C and/or C=O bond of these rings coincide with either the $C_1^1(8)$ chains or with both $C_1^1(6)$ and $C_1^1(8)$ chains. The latter are the two shortest chains in the structure of PDC (longer ones from level 2 are not discussed here). The $C_1^1(6)$ chain includes $\cdots N_{\text{pyr}}-C-C-C-N-H\cdots$. The $C_1^1(8)$ chain runs along $\cdots O=C-C-O-C-C-N-H\cdots$. These chains involve the anti-H atoms of the NH_2 groups, with the cis-H atoms being engaged in the $R_2^2(8)$ rings.

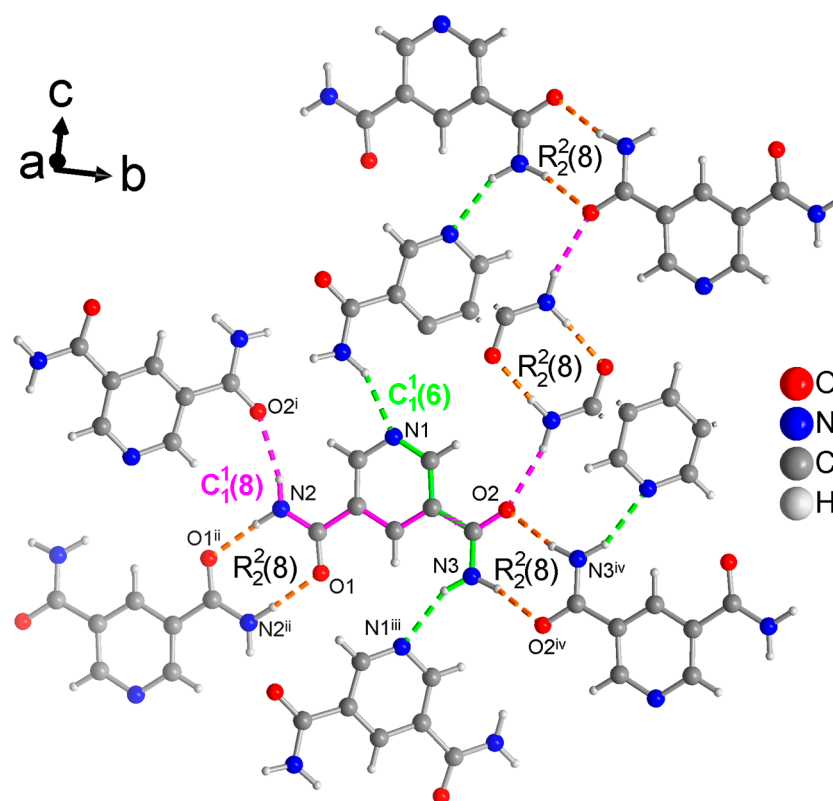


Figure 5. Section of the packing diagram of PDC where the graph-set pattern consists of two different $R_2^2(8)$ rings which are connected by a $C_1^1(6)$ chain (in green) and a $C_1^1(8)$ chain (in pink) such that the $R_2^2(8)$ rings from O1 and N2 are linked by the $C_1^1(8)$ chain and the $R_2^2(8)$ rings from O2 and N3 are linked by the $C_1^1(6)$ chain. Thus, the rings and chains have the same NH_2 donor group. Furthermore, the two different rings are connected by the $C_1^1(8)$ chain (in pink). The hydrogen bonds are depicted as colored dashed lines with the color according to their graph-set assignment. Some molecules have been truncated to avoid overlay. Symmetry codes: (i) $-x + 3/2, y - 1/2, -z + 3/2$; (ii) $-x, -y + 1, -z + 1$; (iii) $x - 1/2, -y + 3/2, z - 1/2$; (iv) $-x + 2, -y + 2, -z + 1$.

For TDC, only one of the symmetry independent amide groups forms a $R_2^2(8)$ ring (Figure 6). The N-C and C=O bonds of this ring are at the same time part of a $C_1^1(4)c$ chain, which expectedly uses the anti-H atom of the NH_2 group. Remarkably, the other amide group does not form a ring but is part of two $C_1^1(4)$ chains. With the anti-H atom, the expected straight $C_1^1(4)a$ chain is formed (cyan in Figure 6). With the syn-H atom, which is normally a part of the $R_2^2(8)$ rings, a second $C_1^1(4)b$ chain is formed (pink in Figure 6) which winds as a 2_1 -helix parallel to the b axis. Note again that longer chains from level 2 are not discussed here.

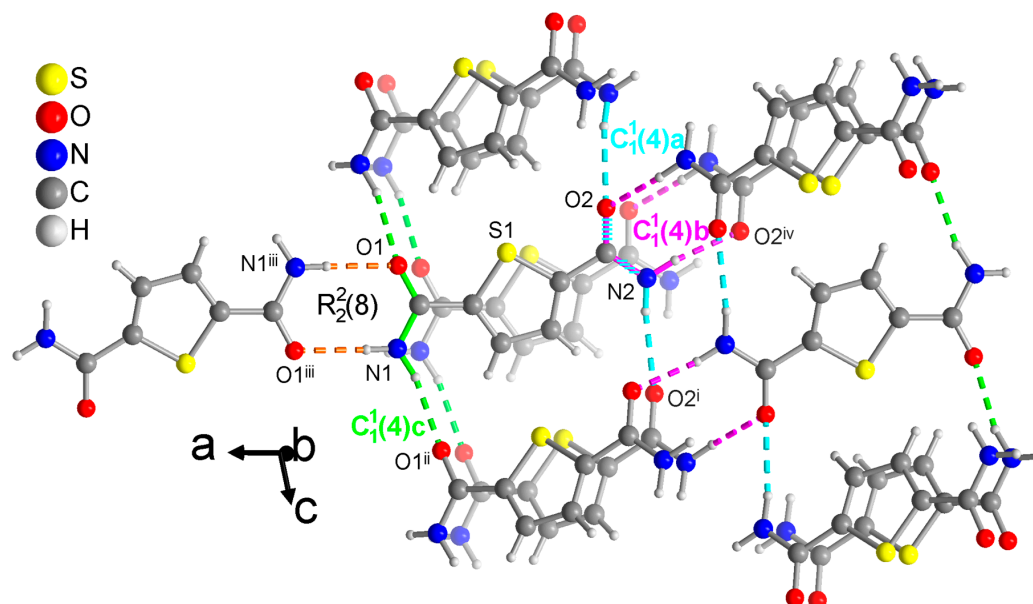


Figure 6. Section of the packing diagram of TDC where the graph-set pattern includes a $R_2^2(8)$ ring which is connected by a $C_1^1(4)$ chain (in green). The second amide group with O2 and N2 does not form a ring but engages in two $C_1^1(4)$ chains (in pink and cyan). The pink $C_1^1(4)$ b chain involves the syn H atom and winds as a 21-helix parallel to the b axis. The cyan and green $C_1^1(4)$ a and c chains which use the anti H atoms run in the c direction. The cyan and pink $C_1^1(4)$ a and b chains share the O-C-N atoms of the same amide group. The hydrogen bonds are depicted as colored dashed lines with the color according to their graph-set assignment. Symmetry codes: (i) $x, -y + 3/2, z + 1/2$; (ii) $x, -y + 1/2, z + 1/2$; (iii) $-x + 2, -y, -z + 1$; (iv) $-x + 1, y + 1/2, -z + 1/2$.

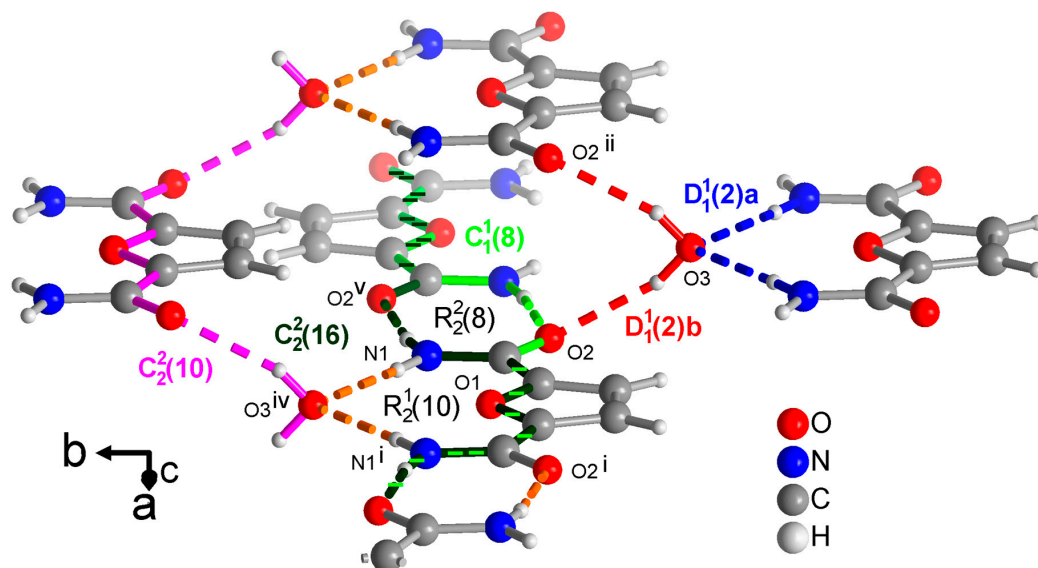


Figure 7. Section of the packing diagram of FDC-solv with graph-set pattern, which contains $R_2^2(8)$ rings alternating with $R_2^1(10)$ rings. The crystal water molecule accepts H bonds from the amino groups and donates to the carboxyl groups in the finite $D_1^1(2)$ a and b patterns (blue and red), respectively. At the same time, the water molecule and the O=C-C-O-C-C=O segment is part of a $C_2^2(10)$ chain (in pink). The chains $C_1^1(8)$ and $C_2^2(16)$ coincide with most of their atoms. The $C_1^1(8)$ chain (in light green) runs along the $\cdots O=C-C-O-C-C-N-H \cdots$ segment. The $C_2^2(16)$ chain (in dark green) has a period of two and involves two FDC molecules with alternating $\cdots O=C-C-O-C-C=O \cdots$ and $\cdots H-N-C-C-O-C-C-N-H \cdots$ segments. The hydrogen bonds are depicted as colored dashed lines with the color according to their graph-set assignment. Symmetry codes: (i) $-x + 2, y, -z + 1/2$; (ii) $-x + 1, y, -z + 1/2$; (iv) $x + 1/2, y + 1/2, z$; (v) $-x + 1, -y + 1, -z + 1$.

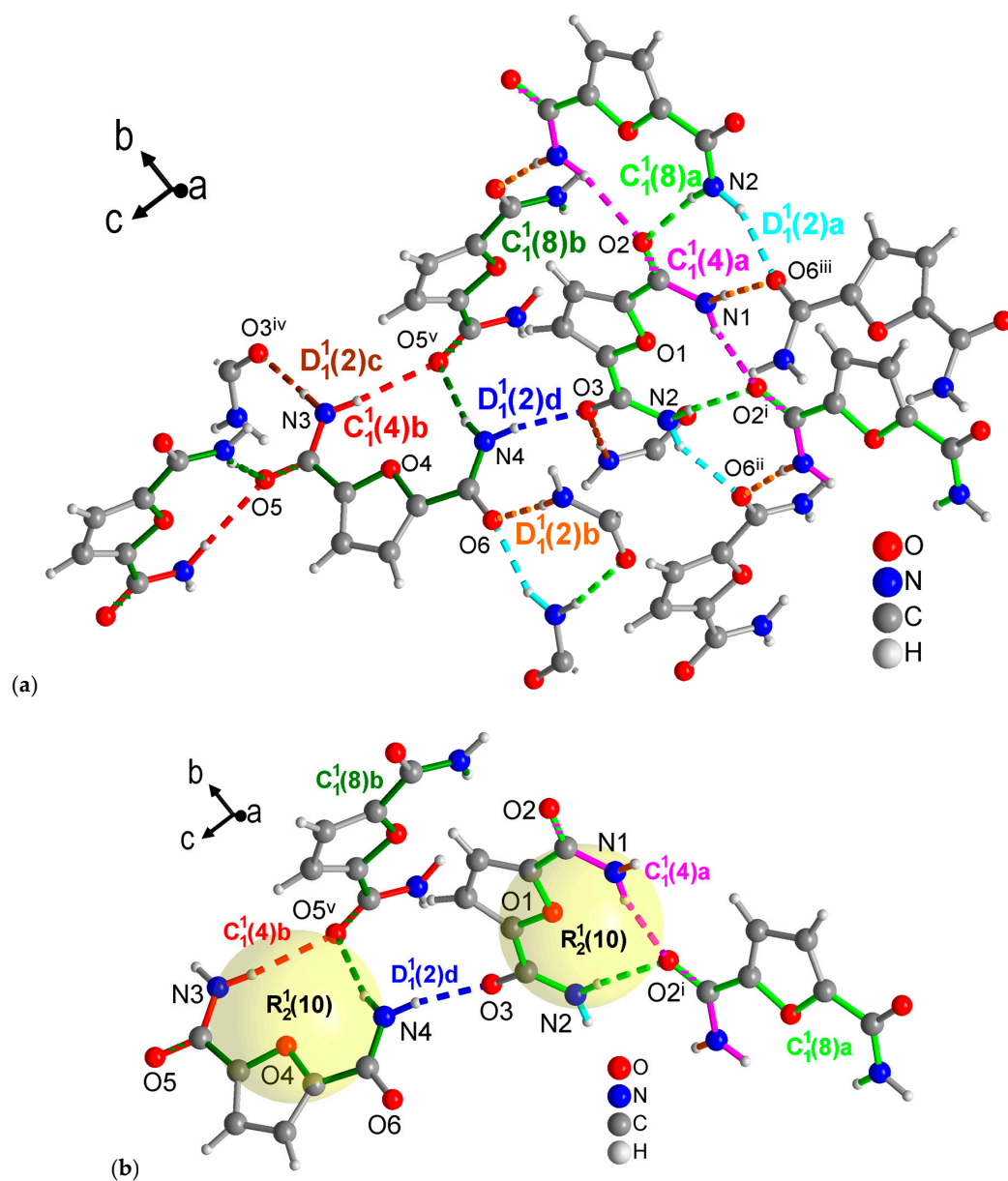


Figure 8. Section of the packing diagrams of FDC-solv with graph-set pattern. (a) Mercury analysis with level 1 graph-sets dissects the H-bonding network into finite $D_1^1(2)$ patterns (differentiated as a, b, c, d given in cyan, orange, brown and blue, respectively) and two different $C_1^1(4)$ chains (a—magenta, b—red) and $C_1^1(8)$ chains (a—light green, b—dark green). Some molecules have been truncated to avoid overlay. (b) Highlighted $R_2^2(10)$ rings as part of the level 2 graph-sets with the rings being also part of the chains segments noted under (a). Symmetry codes: (i) $-x + 2, y - 1/2, -z + 1/2$; (ii) $x, -y + 1/2, z - 1/2$; (iii) $-x + 2, -y + 1, -z + 1$; (iv) $-x + 1, y + 1/2, -z + 3/2$; (v) $x, -y + 3/2, z - 1/2$.

From a methanol solution, FDC-solv crystallizes with a water molecule. This water molecule becomes, of course, part of the H-bonding network as both an acceptor from the NH_2 groups and a donor towards the $\text{C}=\text{O}$ groups in finite $D_1^1(2)$ patterns which are differentiated as a and b in Figure 7. At the same time this crystal water molecule is part of a $C_2^2(10)$ chain (in pink in Figure 7) running along the $\cdots\text{O}=\text{C}-\text{C}-\text{O}-\text{C}-\text{C}=\text{O}\cdots\text{H}-\text{O}-\text{H}\cdots$ part of the FDC molecule. Crystallographically there is only one unique amide group as the FDC molecule has a C_2 axis bisecting the furan ring. This unique amide group forms a $R_2^2(8)$ ring. Across this ring then run a $C_1^1(8)$ and $C_2^2(16)$ chain (in light and dark green, respectively in Figure 7). The shorter $C_1^1(8)$ chain utilizes the $\cdots\text{O}=\text{C}-\text{C}-\text{O}-\text{C}-\text{C}-\text{N}-\text{H}\cdots$ segment. The

longer $C_2^2(16)$ chain (in dark green) extends two FDC molecules with alternating $\cdots O=C-C-O-C-C=O \cdots$ and $\cdots H-N-C-C-O-C-C-N-H \cdots$ segments. Similar long chains also exist in the structures of PDC and TDC as part of the not discussed level 2 graph-sets. For FDC-solv there are no shorter chains so that the above longer chains became part of level 1 graph-sets.

The FDC-subl crystals from sublimation contain two symmetrically independent molecules in the asymmetric unit. This gives rise to four different finite $D_1^1(2)$ patterns, two different $C_1^1(4)$ and $C_1^1(8)$ chains each, which is more than what was seen in the other three structures at level 1 from the Mercury graph-set analysis (Figure 8a). It is noteworthy that unlike the other three structures in this study, FDC-subl does not form the amide-amide $R_2^2(8)$ synthons. At level 2, each independent molecule forms an $R_2^1(10)$ ring with the O=C group of a symmetry-related molecule (Figure 8b).

Unlike the pyridine N-atom in PDC, neither the S-atom in TDC nor the O-atom in both FDC structures become involved in the hydrogen bond network. Yet, the higher negative charge density at the furan-O atom compared to the thiophene-S atom may be responsible for the orientation of both NH_2 groups on the side of the furan-O atom in FDC, whereas the NH_2 groups in TDC are oriented away from the S-atom.

3.3. Hirshfeld Analysis

Hirshfeld surface analysis, conducted using the program CrystalExplorer, was employed to investigate the intermolecular interactions within the crystal structures [51]. This technique involves constructing 3D surface maps based on electron distribution, which facilitates the visualization of close contacts between molecules (Figure 9). In order to identify interactions, additional 2D fingerprint plots were generated (Figure 10) [52,53]. This two-dimensional mapping method uses Hirshfeld surfaces to plot the proportion of surface points against the closest distances to the nuclei inside and outside the surface. Breaking down this fingerprint plot into distinct features allows the identification of specific interactions or contacts ($O \cdots H$, $N \cdots H$, $S \cdots H$, $C \cdots H$, $C \cdots C$ and $H \cdots H$) within the crystal structures of all compounds, thus offering an enhanced understanding of the molecular organization in the crystalline state. The 2D plots with graphical visualizations of the contributions of each interaction for all dicarboxamides can be seen in the Supplementary Materials in Section S7.

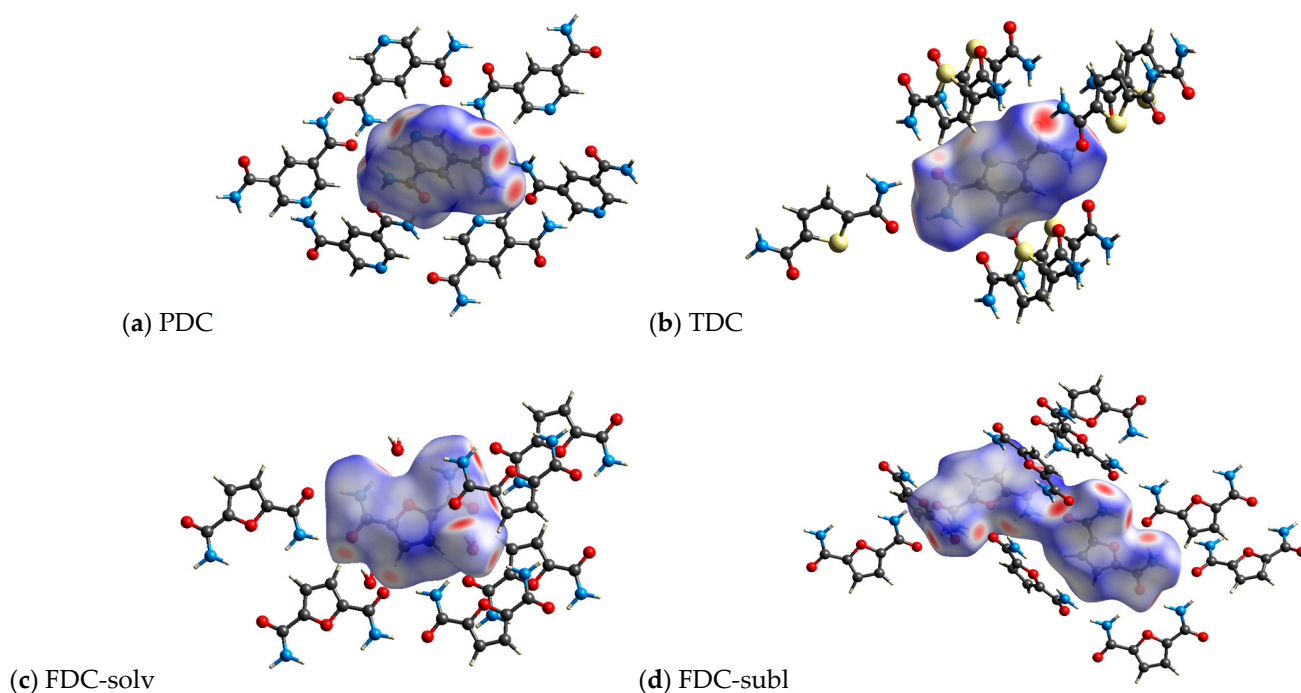


Figure 9. 3D Hirshfeld surface representation of the dicarboxamides plotted over dnorm (a) PDC, (b) TDC, (c) FDC-solv and (d) FDC-subl.

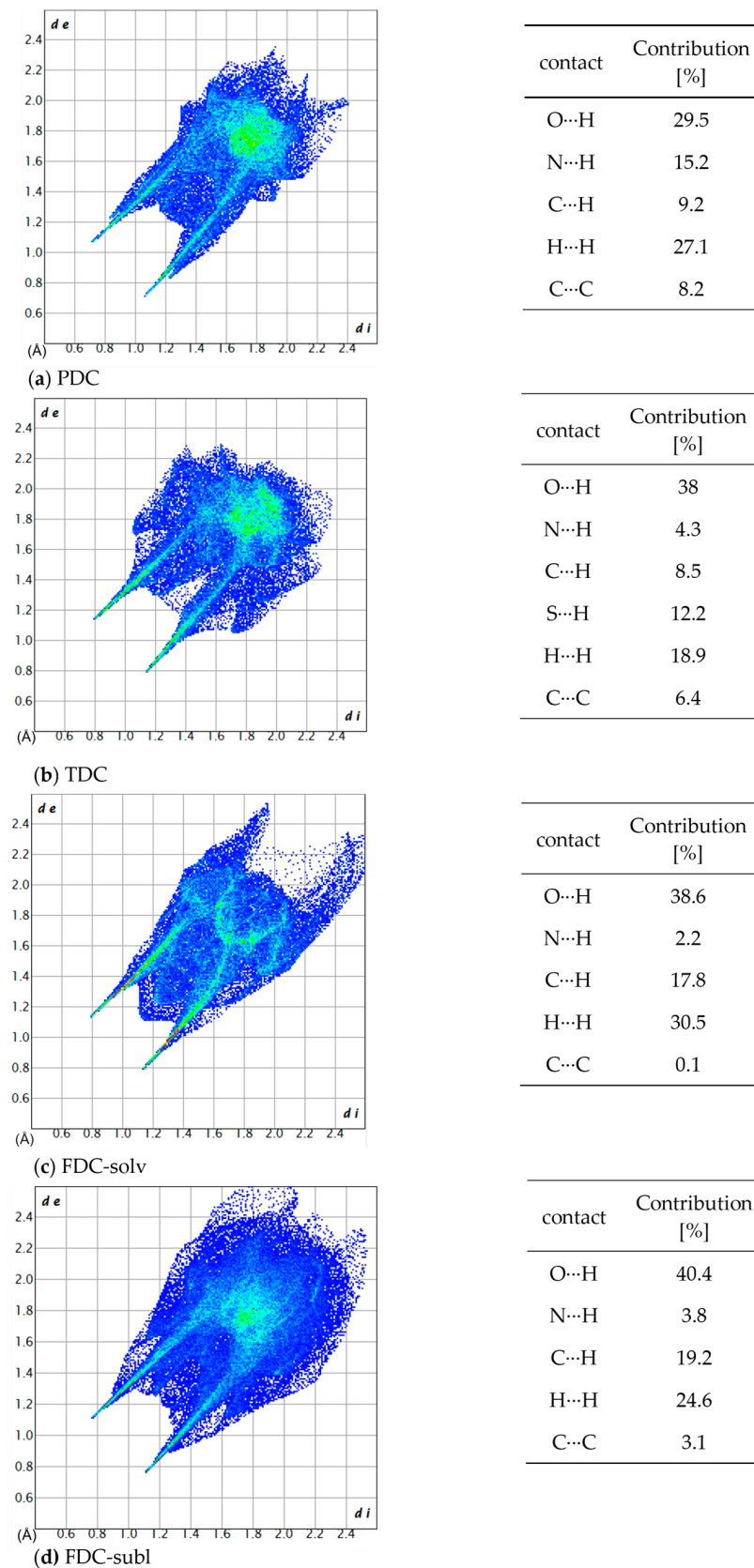


Figure 10. 2D fingerprint plots and the contribution percentage of individual atomic contacts to the Hirshfeld surface of (a) PDC, (b) TDC, (c) FDC-solv and (d) FDC-subl. The spikes pointing to the lower left corner are due to N–H...O/N interactions; d_i and d_e are the distances from the surface to the nearest atom interior and exterior to the surface, respectively.

All investigated dicarboxamides exhibit characteristic spikes in the Hirshfeld 2D plot, confirming the presence of N-H \cdots O hydrogen bonds (Figures S19, S24, S30 and S35). The blue-green lines along these spikes suggest a high proportion of close O \cdots H bond contacts. The dicarboxamides show characteristic spikes extending down to $(d_i, d_e) = (\sim 0.8, \sim 1.1)$, which corresponds to the shortest hydrogen bond distance of 1.9–2.0 Å.

For PDC, this spike shows a broadening due to the contribution of N(pyridine) \cdots H interactions, resulting from the additional hydrogen bonding of the nitrogen atom of the pyridine ring with the closest contact at 2.1 Å $(d_i, d_e) = (0.83, 1.24)$ (Figure S20). The absence of broad wings in PDC explains the significantly lower proportion of C \cdots H interactions (9.2%) (Figure S21). The H \cdots H interactions (27.1%) then cover most of the remaining area in the 2D plot (Figure S22). The intense green area around $d_e = d_i \approx 1.7$ Å stems in part from C \cdots C, that is, $\pi\cdots\pi$ interactions (Figure S20).

For TDC, the pronounced broad wings are not due to C \cdots H interactions (Figure S26) but due to weak S \cdots H interactions ($d_i + d_e \approx 2.8$ Å), which contribute 12.2% to the interactions (Figure S27). H \cdots H interactions (18.9%, Figure S29) cover the central area of the 2D plot, and C \cdots C interactions (Figure S28) contribute to the green area at $d_e = d_i \approx 1.7$ Å.

For FDC-solv, the O \cdots H spikes do not show significant broadening. C \cdots H interactions (17.8%, Figure S32) and H \cdots H contacts (30.5%, Figure S33) fill the body of the 2D plot. Different to PDC and TDC, there are not many interactions (green dots) in the range $d_e = d_i \approx 1.7$ Å.

The O \cdots H spikes of FDC-subl exhibit broadening beyond $(d_i, d_e) = (0.9, 1.3)$ (Figure S35), which can be attributed to O(furan) \cdots H interactions. The 2D plot of FDC-subl exhibits more pronounced wings, primarily due to C \cdots H interactions (19.2%, Figure S37). H \cdots H contacts (24.6%) cover the central part along the diagonal (Figure S38). Also noteworthy, the spread of O \cdots H interactions in FDC-subl is the broadest from $(d_i, d_e) = (\sim 0.75, \sim 1.1)$ to $(\sim 2.1, \sim 2.3)$ (Figure S35).

The carboxamide N atoms are almost within the plane of the attached heterocycle, as measured by the torsion angles C—C—C(=O)—N, which deviate at the most by 11° (in TDC) (Table 8).

Table 8. Torsion angles between amide groups and central aromatic plane of dicarboxamides.

Torsion Angle [°]				
PDC	C—C—C(=O)—N3	7	C—C—C(=O)—N2	2
TDC	C—C—C(=O)—N1	11	C—C—C(=O)—N2	8
FDC-solv	C—C—C(=O)—N1	0.6		
FDC-subl	C—C—C(=O)—N1	6	C—C—C(=O)—N2	3
	C—C—C(=O)—N3	3	C—C—C(=O)—N4	2

3.4. Thermogravimetric Analysis

Thermogravimetric analysis (TGA) was used to assess the temperature stability of the compounds (Figure 11).

For PDC, the TGA curve shows a mass loss of 6% up to 180 °C and a total of 12% up to 240 °C. Starting at 240 °C, a significant mass loss of 82% takes place, followed by complete decomposition at about 550 °C.

TDC exhibits a mass loss of ~7% up to a temperature of 280 °C. Then, after a steep mass decrease, complete decomposition is reached at 350 °C.

With FDC (powder form), a first significant decomposition already occurs at 170 °C reaching a mass loss of 25% at 250 °C, which continues with a steep decrease up to 300 °C with complete decomposition reached at 550 °C.

Additionally, the melting points were determined using an open capillary method. The temperature gradually increased, and the melting of the samples was visually observed. It is notable that all dicarboxamides except for FDC melted within a narrow temperature range followed by subsequent decomposition. The observed melting ranges were 305–307 °C for PDC, 335–337 °C for TDC and 255–262 °C for FDC. The order follows the start of the

decomposition from the TGA. It was also observed that all samples changed the color to brown and shrank before reaching the melting range, indicating decomposition prior to melting.

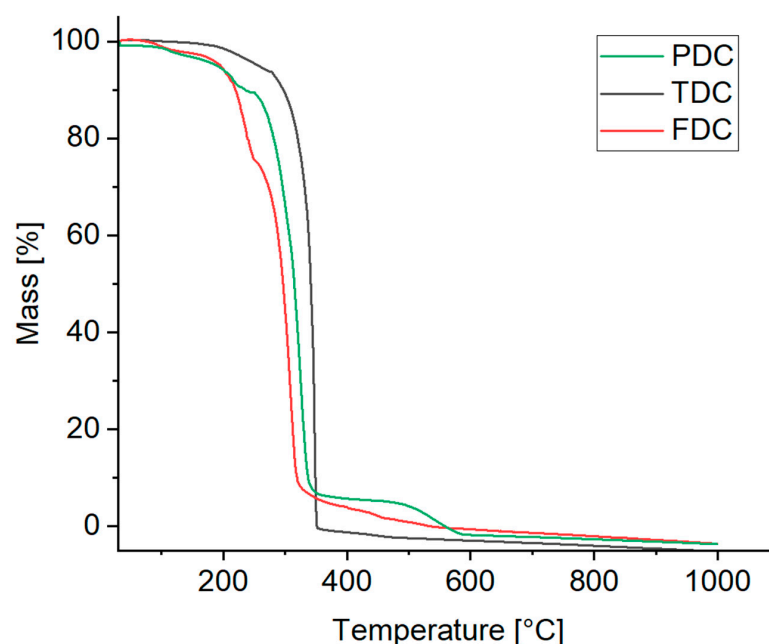


Figure 11. TGA curves of the dicarboxamides (synthetic air, heating rate 10 K min⁻¹).

4. Conclusions

The heteroatom in the aromatic ring of 3,5-pyridinedicarboxamide (PDC) participates in the hydrogen bonding from the amide-NH₂ groups in a C₁¹(6) chain but not the ring heteroatoms in 2,5-thiophenedicarboxamide (TDC) and 2,5-furandicarboxamide (FDC). The reason may be the position of the pyridine-N atom, which is oriented away from the amide-CO acceptors and the more basic nature of the pyridine-N atom in PDC versus the S and O heteroatoms in TDC and FDC. In TDC the less-basic thiophene-S atom is flanked by the amide-CO groups so that they will be the preferred H-acceptor sites. In FDC, the amide-NH₂ groups flank and shield the furan-O atom. It would be interesting to investigate the analogous 3,4-thiophenedicarboxamide and 3,4-furandicarboxamide with more open S and O atoms for participation in the hydrogen-bonding network.

The structures of PDC, TDC and FDC-solv form the head-to-tail R₂²(8) rings together with various chains, such as C₁¹(6) and C₁¹(8) in PDC, several C₁¹(4) chains in TDC and C₁¹(8), C₂²(10) and C₂²(16) in FDC-solv. In PDC and FDC-solv, both amide groups form R₂²(8) rings. It is noteworthy that in TDC only one amide group engages in R₂²(8) ring formation; the other one is part of a 2₁-helical C₁¹(4) chain. The two FDC structures stick out with their syn-NH₂ conformation, which leads to R₂¹(10) rings with the O=C group of a nearby symmetry-related molecule. For the other dicarboxamides, the orientations of the two amide groups with respect to each other are C=O anti NH₂ in PDC and syn-CO and syn-NH₂ in TDC. In TDC the CO groups are on the side of the sulfur heteroatom. The method of crystallization also seems to be important, as FDC-subl contains two symmetry independent molecules in the asymmetric unit which feature two C₁¹(4) and two C₁¹(8) chains, four different finite D₁¹(2) patterns and two R₂¹(10) rings, but surprisingly no R₂²(8) rings.

In summary, dicarboxamide structures with five- and six-membered heterocycles offer a multitude of hydrogen-bond patterns which depend on the role of the heteroatom, the position of the amide groups relative to the heteroatom and the method of crystallization. A description of the hydrogen-bond pattern is best given by its ring, chain or finite elements according to the Etter graph-set formalism.

Supplementary Materials: The following supporting information can be downloaded at: <https://www.mdpi.com/article/10.3390/cryst14090811/s1>, Section S1: Chemicals used; Section S2: Preparation of the dicarboxamides; Section S3: NMR spectra of the dicarboxamides; Section S4: IR spectra of the dicarboxamides; Section S5: Mass spectra of the dicarboxamides; Section S6: PXRD spectra and Le Bail Fitting of the dicarboxamides; Section S7: 2D Hirshfeld plots of the dicarboxamides. Reference [54] is cited in the Supplementary Materials.

Author Contributions: Conceptualization, A.M. and C.J.; methodology, A.M. and I.B.; software, A.M.; validation, A.M., I.B., J.S. and P.S.; formal analysis, A.M., P.S., J.S., I.B. and C.J.; investigation, A.M., J.S., I.B. and P.S.; resources, C.J.; data curation, A.M., P.S., I.B. and J.S.; writing—original draft preparation, A.M.; writing—review and editing, C.J.; visualization, A.M. and C.J.; supervision, C.J. and I.B.; project administration, C.J.; funding acquisition, C.J. All authors have read and agreed to the published version of the manuscript.

Funding: Deutsche Forschungsgemeinschaft (DFG) under grant 440366605 (for the Rigaku diffractometer).

Data Availability Statement: The data presented in this study are available on request from the corresponding author. The CCDC numbers 2374614–2374617 for compounds PDC, TDC, FDC-solv and FDC-subl contain the supplementary crystallographic data reported in this paper. These data can be obtained free of charge from the Cambridge Crystallographic Data Centre via www.ccdc.cam.ac.uk/data_request/cif (accessed on 25 August 2024).

Acknowledgments: The authors would like to thank Birgit Tommes for the IR measurements, István Boldog for his continuous help and the instructive crystallography course. István Boldog is only responsible for the project formulation, synthetic/crystallization supervision and crystallographic troubleshooting. We also thank the Center for Molecular and Structural Analytics at Heinrich Heine University (CeMSA@HHU) for recording the mass spectrometric and NMR-spectrometric data.

Conflicts of Interest: The authors declare no conflict of interest.

References

1. Sewald, N.; Jakubke, H.D. *Peptides: Chemistry and Biology*; Wiley-VCH: Weinheim, Germany, 2002.
2. Kumari, S.; Carmona, A.V.; Tiwari, A.K.; Trippier, P.C. Amide bond bioisosteres: Strategies, synthesis, and successes. *J. Med. Chem.* **2020**, *63*, 12290–12358. [[CrossRef](#)] [[PubMed](#)]
3. Johansson, A.; Kollman, P.; Rothenberg, S.; McKelvey, J. Hydrogen bonding ability of the amide group. *J. Am. Chem. Soc.* **1974**, *96*, 3794–3800. [[CrossRef](#)]
4. Hutchins, K.M. Functional materials based on molecules with hydrogen-bonding ability: Applications to drug co-crystals and polymer complexes. *R. Soc. Open Sci.* **2018**, *5*, 180564. [[CrossRef](#)] [[PubMed](#)]
5. Shi, J.; Xiao, Z.; Kamaly, N.; Farokhzad, O.C. Self-assembled targeted nanoparticles: Evolution of technologies and bench to bedside translation. *Acc. Chem. Res.* **2011**, *44*, 1123–1134. [[CrossRef](#)]
6. Tibbitt, M.W.; Dahlman, J.E.; Langer, R. Emerging frontiers in drug delivery. *J. Am. Chem. Soc.* **2016**, *138*, 704–717. [[CrossRef](#)]
7. Wang, J.; Li, Y.; Nie, G. Multifunctional biomolecule nanostructures for cancer therapy. *Nat. Rev. Mater.* **2021**, *6*, 766–783. [[CrossRef](#)]
8. Panda, C.; Sarkar, A.; Gupta, S.S. Coordination chemistry of carboxamide 'N_x' ligands to metal ions for bio-inspired catalysis. *Coord. Chem. Rev.* **2020**, *417*, 213314. [[CrossRef](#)]
9. Kumar, V.; Kumar, P.; Gupta, R. Detection of Al³⁺ and Fe³⁺ ions by nitrobenzoxadiazole bearing pyridine-2, 6-dicarboxamide based chemosensors: Effect of solvents on detection. *New J. Chem.* **2020**, *44*, 13285–13294. [[CrossRef](#)]
10. Rahimi, H.; Hosseinzadeh, R.; Tajbakhsh, M. A new and efficient pyridine-2,6-dicarboxamide-based fluorescent and colorimetric chemosensor for sensitive and selective recognition of Pb²⁺ and Cu²⁺. *J. Photochem. Photobiol. A Chem.* **2021**, *407*, 113049. [[CrossRef](#)]
11. Geng, W.-C.; Jiang, Z.-T.; Chen, S.-L.; Guo, D.-S. Supramolecular interaction in the action of drug delivery systems. *Chem. Sci.* **2024**, *15*, 7811–7823. [[CrossRef](#)]
12. Bernhard, S.; Tibbitt, M.W. Supramolecular engineering of hydrogels for drug delivery. *Adv. Drug Deliv. Rev.* **2021**, *171*, 240–256. [[CrossRef](#)]
13. Deng, C.-L.; Murkli, S.L.; Isaacs, L.D. Supramolecular hosts as in vivo sequestration agents for pharmaceuticals and toxins. *Chem. Soc. Rev.* **2020**, *49*, 7516–7532. [[CrossRef](#)]
14. Yan, M.; Wu, S.; Wang, Y.; Liang, M.; Wang, M.; Hu, W.; Yu, G.; Mao, Z.; Huang, F.; Zhou, J. Recent progress of supramolecular chemotherapy based on host–guest interactions. *Adv. Mater.* **2024**, *36*, 2304249. [[CrossRef](#)] [[PubMed](#)]
15. Caro Garrido, C.; Vandooen, M.; Robeyns, K.; Debecker, D.P.; Luis, P.; Leyssens, T. Combining a Drug and a Nutraceutical: A New Cocrystal of Praziquantel and Curcumin. *Crystals* **2024**, *14*, 181. [[CrossRef](#)]
16. Lehn, J.-M. Perspectives in chemistry—Steps towards complex matter. *Angew. Chem. Int. Ed.* **2013**, *52*, 2836–2850. [[CrossRef](#)]

17. Pauling, L. The nature of the chemical bond. II. The one-electron bond and the three-electron bond. *J. Am. Chem. Soc.* **1931**, *53*, 3225–3237. [[CrossRef](#)]
18. Desiraju, G.R. Supramolecular synthons in crystal engineering—A new organic synthesis. *Angew. Chem. Int. Ed.* **1995**, *34*, 2311–2327. [[CrossRef](#)]
19. Steiner, T. The hydrogen bond in the solid state. *Angew. Chem. Int. Ed.* **2002**, *41*, 48–76. [[CrossRef](#)]
20. Etter, M.C. Encoding and decoding hydrogen-bond patterns of organic compounds. *Acc. Chem. Res.* **1990**, *23*, 120–126. [[CrossRef](#)]
21. Etter, M.C. Aggregate structures of carboxylic acids and amides. *Isr. J. Chem.* **1985**, *25*, 312–319. [[CrossRef](#)]
22. Etter, M.C. Hydrogen bonds as design elements in organic chemistry. *J. Phys. Chem.* **1991**, *95*, 4601–4610. [[CrossRef](#)]
23. Boéré, R.T. Hydrogen Bonds Stabilize Chloroselenite Anions: Crystal Structure of a New Salt and Donor-Acceptor Bonding to SeO₂. *Molecules* **2023**, *28*, 7489. [[CrossRef](#)]
24. Ejarque, D.; Calvet, T.; Font-Bardia, M.; Pons, J. Cocrystals based on 4, 4'-bipyridine: Influence of crystal packing on melting point. *Crystals* **2021**, *11*, 191. [[CrossRef](#)]
25. Bojarska, J.; Łyczko, K.; Mieczkowski, A. Synthesis, Crystal Structure and Supramolecular Features of Novel 2, 4-Diaminopyrimidine Salts. *Crystals* **2024**, *14*, 133. [[CrossRef](#)]
26. Bojarska, J.; Łyczko, K.; Breza, M.; Mieczkowski, A. Recurrent Supramolecular Patterns in a Series of Salts of Heterocyclic Polyamines and Heterocyclic Dicarboxylic Acids: Synthesis, Single-Crystal X-ray Structure, Hirshfeld Surface Analysis, Energy Framework, and Quantum Chemical Calculations. *Crystals* **2024**, *14*, 733. [[CrossRef](#)]
27. Iwanek, E.M.; Gliński, M. Study of the Influence of the Change from Methyl to Isopropyl Substituents in 1-(2,4,6-trialkylphenyl) ethanol on the Point Group Symmetry of the 0-D Hydrogen-Bonded Moiety. *Crystals* **2024**, *14*, 642. [[CrossRef](#)]
28. Baishya, T.; Dutta, K.K.; Frontera, A.; Gomila, R.M.; Barceló-Oliver, M.; Bhattacharyya, M.K. On the Importance of H-Bonding Interactions in the Enclathration of Boric Acids in Na (I) Polymers: Experimental and Theoretical Studies. *Crystals* **2023**, *13*, 895. [[CrossRef](#)]
29. Bernstein, J.; Davis, R.E.; Shimoni, L.; Chang, N.-L. Patterns in hydrogen bonding: Functionality and graph-set analysis in crystals. *Angew. Chem. Int. Ed.* **1995**, *34*, 1555–1573. [[CrossRef](#)]
30. Desiraju, G.R.; Steiner, T. *The Weak Hydrogen Bond in Structural Chemistry and Biology*; Oxford University Press: Oxford, UK, 1999.
31. Leiserowitz, L.; Schmidt, G.M. Molecular packing modes. Part III. Primary amides. *J. Chem. Soc. A* **1969**, 2372–2382. [[CrossRef](#)]
32. Macrae, C.F.; Sovago, I.; Cottrell, S.J.; Galek, P.T.A.; McCabe, P.; Pidcock, E.; Platings, M.; Shields, G.P.; Stevens, J.S.; Towler, M.; et al. Mercury 4.0: From visualization to analysis, design and prediction. *J. Appl. Crystallogr.* **2020**, *53*, 226–235. [[CrossRef](#)]
33. Usha, R.; Venkatesan, K. The structure of cyclopropane-1, 1-dicarboxamide. *Acta Crystallogr. B.* **1979**, *35*, 2730–2732. [[CrossRef](#)]
34. Baudron, S.A.; Avarvari, N.; Batail, P.; Coulon, C.; Clérac, R.; Canadell, E.; Auban-Senzier, P. Singular Crystalline β'-Layered Topologies Directed by Ribbons of Self-Complementary Amide ··· Amide Ring Motifs in [EDT-TTF-(CONH₂)₂]₂X (X = HSO₄⁻, ClO₄⁻, ReO₄⁻, AsF₆⁻): Coupled Activation of Ribbon Curvature, Electron Interactions, and Magnetic Susceptibility. *J. Am. Chem. Soc.* **2003**, *125*, 11583–11590. [[CrossRef](#)] [[PubMed](#)]
35. Marlin, D.S.; Olmstead, M.M.; Mascharak, P.K. Extended structures controlled by intramolecular and intermolecular hydrogen bonding: A case study with pyridine-2, 6-dicarboxamide, 1, 3-benzenedicarboxamide and N, N-dimethyl-2, 6-pyridinedicarboxamide. *J. Mol. Struct.* **2000**, *554*, 211–223. [[CrossRef](#)]
36. Cobblestick, R.E.; Small, R.W. The crystal structure of terephthalamide. *Acta Crystallogr. B.* **1972**, *28*, 2893–2896. [[CrossRef](#)]
37. Meyer, H.; Tropsch, H. Zur Kenntnis der Polymerie bei Pyridincarbonsäurechloriden. *Monatshfte Für Chem.* **1914**, *35*, 783–784. [[CrossRef](#)]
38. Oussaid, B.; Fayet, J.-P.; Pelletier, G.; Garrigues, B. Etude De La Conformation D'oximes Thiopheniques. *Bull. Soc. Chim. Belg.* **1992**, *101*, 969–975. [[CrossRef](#)]
39. Klinkhardt, A. Derivate und Zersetzungsprodukte der Schleimsäure und Dehydroschleimsäure. *J. Prakt. Chem.* **1882**, *25*, 41–59. [[CrossRef](#)]
40. Meyer, H.; McArdle, P.; Erxleben, A. Sublimation—a green route to new solid-state forms. *CrystEngComm* **2021**, *23*, 5965–5975. [[CrossRef](#)]
41. Salzillo, T.; Della Valle, R.G.; Venuti, E.; Brillante, A.; Siegrist, T.; Masino, M.; Mezzadri, F.; Girlando, A. Two new polymorphs of the organic semiconductor 9,10-diphenylanthracene: Raman and X-ray analysis. *J. Phys. Chem. C* **2016**, *120*, 1831–1840. [[CrossRef](#)]
42. Smith, V.J.; Marais, C.G.; Suwińska, K.; Lipkowski, J.; Szumna, A.; Esterhuysen, C.; Barbour, L.J. Concomitant polymorphs of p-iso-propylcalix[4]arene. *CrystEngComm* **2015**, *17*, 5129–5133. [[CrossRef](#)]
43. CrysAlisPro. *Rigaku Oxford Diffraction*; Release 1.171.40.103a; Agilent Technologies Ltd.: Yarnton, UK, 2014; Available online: https://scholar.google.com/scholar_lookup?title=Rigaku+Oxford+Diffraction&author=CrysAlisPro&publication_year=2014 (accessed on 30 July 2024).
44. Dolomanov, O.V.; Bourhis, L.J.; Gildea, R.J.; Howard, J.A.K.; Puschmann, H. OLEX2: A complete structure solution, refinement and analysis program. *J. Appl. Crystallogr.* **2009**, *42*, 339–341. [[CrossRef](#)]
45. Sheldrick, G.M. SHELXT—Integrated space-group and crystal-structure determination. *Acta Crystallogr. A* **2015**, *71*, 3–8. [[CrossRef](#)] [[PubMed](#)]
46. Sheldrick, G.M. Crystal structure refinement with SHELXL. *Acta Crystallogr. C* **2015**, *71*, 3–8. [[CrossRef](#)] [[PubMed](#)]
47. Brandenburg, K. *Diamond, Version 5.0.0*; Crystal and Molecular Structure Visualization, Crystal Impact; K. Brandenburg & H. Putz Gbr: Bonn, Germany, 2023.

48. Lu, T.; Chen, F. Multiwfn: A multifunctional wavefunction analyzer. *J. Comput. Chem.* **2012**, *33*, 580–592. [[CrossRef](#)]
49. Frisch, M.J.; Trucks, G.W.; Schlegel, H.B.; Scuseria, G.E.; Robb, M.A.; Cheeseman, J.R.; Scalmani, G.; Barone, V.; Petersson, G.A.; Nakatsuji, H.; et al. *Gaussian 16, Revision C.01*; Gaussian, Inc.: Wallingford, CT, USA, 2016.
50. Wu, Y.Y.; Meng, M.; Wang, G.Y.; Feng, P.; Liu, C.Y. Optically probing the localized to delocalized transition in Mo₂–Mo₂ mixed-valence systems. *Chem. Commun.* **2017**, *53*, 3030–3033. [[CrossRef](#)]
51. Spackman, P.R.; Turner, M.J.; McKinnon, J.J.; Wolff, S.K.; Grimwood, D.J.; Jayatilaka, D.; Spackman, M.A. CrystalExplorer: A program for Hirshfeld surface analysis, visualization and quantitative analysis of molecular crystals. *J. Appl. Crystallogr.* **2021**, *54*, 1006–1011. [[CrossRef](#)]
52. McKinnon, J.J.; Jayatilaka, D.; Spackman, M.A. Towards quantitative analysis of intermolecular interactions with Hirshfeld surfaces. *Chem. Commun.* **2007**, 3814–3816. [[CrossRef](#)]
53. Spackman, M.A.; McKinnon, J.J. Fingerprinting intermolecular interactions in molecular crystals. *CrystEngComm* **2002**, *4*, 378–392. [[CrossRef](#)]
54. Petříček, V.; Dušek, M.; Palatinus, L. Crystallographic computing system JANA2006: General features. *Z. Kristallogr.-Cryst. Mater.* **2014**, *229*, 345–352. [[CrossRef](#)]

Disclaimer/Publisher’s Note: The statements, opinions and data contained in all publications are solely those of the individual author(s) and contributor(s) and not of MDPI and/or the editor(s). MDPI and/or the editor(s) disclaim responsibility for any injury to people or property resulting from any ideas, methods, instructions or products referred to in the content.